

Dalton Transactions

Accepted Manuscript



This is an *Accepted Manuscript*, which has been through the Royal Society of Chemistry peer review process and has been accepted for publication.

Accepted Manuscripts are published online shortly after acceptance, before technical editing, formatting and proof reading. Using this free service, authors can make their results available to the community, in citable form, before we publish the edited article. We will replace this *Accepted Manuscript* with the edited and formatted *Advance Article* as soon as it is available.

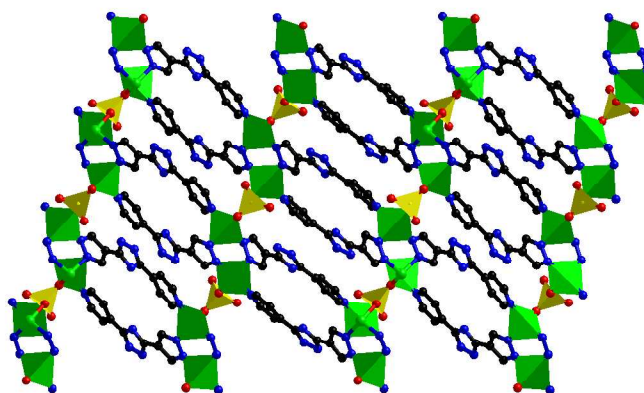
You can find more information about *Accepted Manuscripts* in the [Information for Authors](#).

Please note that technical editing may introduce minor changes to the text and/or graphics, which may alter content. The journal's standard [Terms & Conditions](#) and the [Ethical guidelines](#) still apply. In no event shall the Royal Society of Chemistry be held responsible for any errors or omissions in this *Accepted Manuscript* or any consequences arising from the use of any information it contains.

An Acid - Stable Zn (II) Complex: Electrodeposition in Sulfuric Acid and the Effect on Zinc - Lead Dioxide Battery

Miao Miao Zhang, Yun Gong,^{*} Pan Zhang, Hui Fang Shi and Jian Hua Lin^{*}

An acid-stable Zn(II) complex with a 3D dense architecture can be synthesized hydrothermally or via electrodeposition in sulfuric acid.



An acid - stable Zn (II) complex: electrodeposition in sulfuric acid and the effect on zinc - lead dioxide battery

Miao Miao Zhang,^a Yun Gong,^{*a} Pan Zhang,^a Hui Fang Shi^a and Jian Hua Lin^{*a,b}

^aDepartment of Applied Chemistry, College of Chemistry and Chemical Engineering, Chongqing University, Chongqing 400030, P. R. China Tel: +86-023-65106150 E-mail: gongyun7211@cqu.edu.cn

^bZhejiang University, Hangzhou 310058, P. R. China Tel: +86-0571-88981583 E-mail: jhlin@zju.edu.cn; jhlin@cqu.edu.cn; jhlin@pku.edu.cn

*This submission was created using the RSC Article Template (DO NOT DELETE THIS TEXT)
(LINE INCLUDED FOR SPACING ONLY - DO NOT DELETE THIS TEXT)*

An acid - stable Zn (II) complex formulated as $Zn_2(HL)_2(SO_4) \cdot H_2O$ (**1**) and an acid - unstable complex formulated as $Zn_2L_2 \cdot 12H_2O$ (**2**) have been hydro(solvo)thermally synthesized and structurally characterized by single-crystal X - ray diffraction. Complex **1** features a uninodal 6 - connected 2 - fold interpenetrating three - dimensional (3D) dense architecture with $\{4^{12} \cdot 6^3\}$ - **pcu** topology, and complex **2** exhibits a 2 - nodal (3, 6) - connected 3D open architecture with $(4 \cdot 6^2)_2(4^2 \cdot 6^{10} \cdot 8^3)$ - **rtl** topology. The example indicates the stability of complex **1** in sulfuric acid is probably associated with the coordinated SO_4^{2-} in the quite dense structure. And complex **1** also can be synthesized via electrodeposition in sulfuric acid, it can improve the discharging characteristics of zinc - lead dioxide battery under room temperature.

Introduction

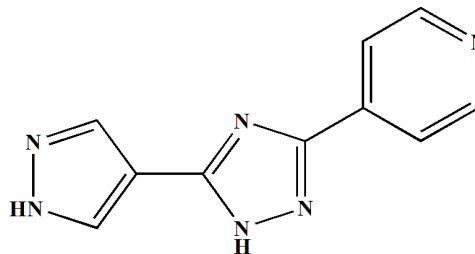
Coordination polymers (CPs), are crystalline materials consisting of metal ions, or metal ion clusters and organic ligands, which are linked together to form extended frameworks. Over the last decade, porous CPs have received widespread attention owing to their potential applications in gas storage, separation, and catalysis, et al.¹ Among the varied metal and ligand combinations that have been investigated, Zn (II) - based CPs have been the most widely studied due to their many favorable attributes and the easily accessible resource of Zn (II).² However, many zinc-carboxylate CPs are prone to breakdown in the presence of water or protic solvents,³ which greatly limits their application in aqueous or acidic medium.

In order to obtain stable and chemically - resistant frameworks, different metal ions and organic ligands have been explored. For example, the use of more oxophilic, high oxidation state metal ions such as Zr (IV) in UiO - 66,⁴ or kinetically inert metal ions such as Cr (III) in MIL - 101.⁵ Zeolite - like porous structures have been constructed by imidazole and metal (II), which was reported to be tolerant to moisture, making the porous zeolitic imidazolate frameworks (ZIFs) rather attractive for industrial applications.⁶ The better water stability of the nitrogen-coordinated CPs than the carboxylate based CPs,^{3b,7} is probably attributed to the higher basicity of the N - donor relative to the carboxylate ligand. It is expected that the metal, being a Lewis acid, will form a stronger bond with the more basic ligand to obtain more water-stable CPs.⁷

With the depletion of fossil fuels, the technology associated with energy conversion and storage has drawn researchers' more and more interests. Aqueous acid electrolyte such as H_2SO_4 , which possesses high ion mobility, is usually used in battery such as lead - acid and Zn - PbO_2 batteries. As a prerequisite to be used in the electrochemical field, exceptional stability in H_2SO_4 aqueous solution is required for the CPs.

Based on the situation, herein, we synthesized a N - donating ligand, 4-(5-(1H-pyrazol-4-yl)-1H-1,2,4-triazol-3-yl)pyridine (**H₂L**) (Scheme 1).⁸ The ligand attracts our interest based on the following considerations: 1) **H₂L** possesses three kinds of N - donor groups, pyrazole, 1, 2, 4 - triazole and pyridine rings. The higher basicity of the N - donor relative to the carboxylate ligand makes the N - donating ligand a suitable candidate for the

construction of water - stable CP; 2) In the structure of the ligand, two mobile H atoms are attached to the pyrazol and triazol N atoms, respectively. However, the ligand possesses six N atoms, which is more than the number of the mobile H atoms, allowing the ligand can function as a proton reservoir, accept proton and exhibit acid tolerance; 3) Based on the principle of electroneutrality that all pure substances fulfill, in the crystalline phase all positive charges must be compensated by negative counter charges. The positive charge on the metal centre is either balanced by the negative charge on the organic ligand or a third anionic component. Here, the pyridine group of the ligand (Scheme 1) can combine metal ions in the neutral form, making it possible to introduce anionic SO_4^{2-} into the structure of the CP. If SO_4^{2-} is one of the components of the CP, maybe the CP is stable in the sulfate solution. In the present work, hydrothermal reaction of $ZnSO_4$ with **H₂L** yields a novel CP formulated as $Zn_2(HL)_2(SO_4) \cdot H_2O$ (**1**) in moderate yield. For comparison, in the absence of SO_4^{2-} , another CP formulated as $Zn_2L_2 \cdot 12H_2O$ (**2**) was solvothermally synthesized. The electrochemical property, UV-visible spectra, electrodeposition for complex **1**, the effect of complex **1** on the discharge of the Zn - PbO_2 battery, and the thermal stabilities of the two complexes have been investigated.



Scheme 1 Schematic representation of **H₂L**.

Experimental

General Considerations

All chemicals purchased were of reagent grade and used without further purification. The melting point was determined using an uncorrected X-4 melting point apparatus of Beijing Kaifu Company. C, H, N elemental analyses were performed on

an Elementar Vario MICRO E III analyzer. IR spectra were recorded as KBr pellets on a Nicolet iS50 FT-IR spectrometer. The powder XRD (PXRD) data were collected on a RIGAKU DMAX2500PC diffractometer using Cu K α radiation. UV-Vis spectra were measured on a HITACHI U-4100 UV-vis spectrophotometer. TGA was performed on a NETZSCH STA 449C thermogravimetric analyzer in flowing N₂ with a heating rate of 10°C·min⁻¹.

Electrochemical Measurements

The electrochemical measurements were done in a three-electrode test cell with a saturated calomel electrode (SCE) and a platinum foil as the reference and counter electrode, respectively. 4 mg complex **1** was ultrasonicated in a mixture of acetone (1 mL) and nafion (0.05 mL) solution, then was deposited on a glassy carbon electrode with a 0.2 cm² of the geometrical area to obtain the working electrodes after the solvent is dried by an IR lamp. The electrodes were immersed in 0.5 M H₂SO₄ aqueous solution (50 mL) and a Shiruisi RST5200 electrochemical workstation was used for the electrochemical measurements. The galvanostatic discharge measurements were conducted on a Neware BTS-5V5mA battery analyzer in a two-electrode cell, in which a 4 mg Zn powder modified GCE (**Zn - GCE**) and a 4 mg PbO₂ powder modified GCE (**PbO₂ - GCE**) were used as negative and positive electrodes, respectively. And the 0.5 M H₂SO₄ aqueous solution (50 mL) was used as electrolyte.

Synthesis

Synthesis of H₂L: H₂L was prepared according to the literature method.⁹ Melting point: >250 °C. IR (cm⁻¹): 3396 (m), 3124 (s), 3064 (s), 2995 (s), 2677 (s), 1852 (m), 1635 (s), 1612 (s), 1510 (w), 1421 (s), 1350 (s), 1290 (s), 1256 (m), 1151 (s), 1055 (s), 1009 (s), 941 (s), 857 (s), 837 (s), 750 (s), 712 (s), 627 (w), 527 (w).

Synthesis of Zn₂(HL)₂(SO₄)·H₂O (1): A mixture of ZnSO₄·7H₂O (0.05 mmol, 0.014 g), H₂L (0.025 mmol, 0.005 g), water (8 mL) and NH₃·H₂O (0.1 mL) was sealed in a Teflon-lined autoclave and heated at 120 °C for 3 days, then followed by slow cooling to room temperature. The resulting colorless block crystals were filtered off (yield: ca. 72 % based on H₂L). Elemental Anal. Found: C, 36.01; H, 2.43; N, 25.17 %. Calcd. For Zn₂C₂₀H₁₆N₁₂O₅S: C, 36.00; H, 2.42; N, 25.19 %. IR (cm⁻¹): 3408 (s), 3159 (s), 3084 (s), 2999 (s), 2820 (s), 1628 (s), 1518 (s), 1435 (s), 1369 (s), 1304 (s), 1263 (m), 1202 (s), 1178 (s), 1128 (s), 1063 (s), 1042 (s), 941 (m), 845 (m), 756 (m), 633 (w), 546 (w).

Synthesis of Zn₂L₂·12H₂O (2): The synthesis of complex **2** was carried out as described above for complex **1**, but starting with the mixture of Zn(NO₃)₂·7H₂O (0.075 mmol, 0.022 g), H₂L (0.025 mmol, 0.005 g) and DMF (8 mL). The yield of the colorless block crystals is ca. 68 % based on H₂L. Elemental Anal. Found: C, 31.52; H, 4.84; N, 21.79 %. Calcd. for Zn₂C₂₀H₃₆N₁₂O₁₂: C, 31.30; H, 4.73; N, 21.90 %. IR (cm⁻¹): 3395 (s), 1656 (s), 1623 (s), 1447 (s), 1386 (m), 1296 (m), 1278 (s), 1084 (m), 1053 (s), 1031 (m), 1000 (s), 955 (m), 872 (m), 844 (m), 761 (m), 709 (m), 667 (w).

X-ray crystallography

Single - crystal X - ray data for complexes **1** and **2** were collected on a SuperNova diffractometer using graphite monochromated Mo K α (λ = 0.71073 Å) radiation at room temperature. Empirical absorption correction was applied. The structures were solved by direct methods and refined by the full-

matrix least-squares methods on F^2 using the SHELXTL-97 software.¹⁰ All non-hydrogen atoms were refined anisotropically. Hydrogen atoms attached to N3, N10 and O5 in complex **1** were located in the Fourier difference maps. All of the other hydrogen atoms were placed in the calculated positions. The solvent molecule in complex **2** was highly disordered and was impossible to refine using conventional discrete-atom models, thus the contribution of partial solvent electron densities were removed by the SQUEEZE routine in PLATON.¹¹ The final chemical formula of complex **2** was estimated from the SQUEEZE result combined with the TGA result. The crystal data and structure refinements for complexes **1** and **2** are summarized in **Table 1**. Selected bond lengths and angles for complexes **1** and **2** are listed in **Table S1** in the supporting information. The CCDC reference numbers are the following: 984658 for complex **1** and 984659 for complex **2**.

Table 1 Crystal data and structure refinements for complexes **1** and **2**

Complex	1	2
Empirical formula	Zn ₂ C ₂₀ H ₁₆ N ₁₂ O ₅ S	Zn ₂ C ₂₀ H ₃₆ N ₁₂ O ₁₂
M	667.25	767.39
Crystal system	monoclinic	monoclinic
Space group	$P2_1/c$	$P2_1/c$
$a/\text{Å}$	11.7747(5)	7.2259(2)
$b/\text{Å}$	15.2659(5)	18.6983(6)
$c/\text{Å}$	14.3648(6)	15.1420(6)
$\alpha/^\circ$	90	90
$\beta/^\circ$	108.979(4)	93.144(3)
$\gamma/^\circ$	90	90
$V/\text{Å}^3$	2441.72(17)	2042.80(13)
Z	4	2
$D_{\text{calc}}/\text{g cm}^{-3}$	1.815	0.925
μ/mm^{-1}	2.112	1.197
No. of unique reflens	4269	3605
reflens used [$I > 2\sigma(I)$]	3768	3182
$F(0\ 0\ 0)$	1344	572
Goodness-of-fit on F^2	1.042	1.091
Final R indices	$R_1 = 0.0293$, $wR_2 = 0.0706$	$R_1 = 0.0419$, $wR_2 = 0.1444$

$$R_1 = \sum |F_o - F_c| / \sum F_o; wR_2 = \sum [w(F_o^2 - F_c^2)^2] / \sum [w(F_o^2)^2]^{1/2}$$

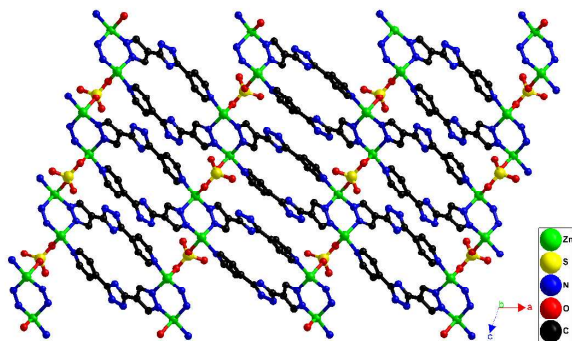
Results and discussion

Crystal Structure of Zn₂(HL)₂(SO₄)·H₂O (1) Single-crystal X-ray diffraction analysis reveals that complex **1** crystallizes in the *monoclinic* space group $P2_1/c$ (**Table 1**) with two Zn (II), two HL⁻, one SO₄²⁻ and one uncoordinated water molecule in the asymmetric unit. The crystallographically independent Zn (1) and Zn (2) show a similar slightly distorted tetrahedral coordination geometry, being coordinated by two pyrazol N atoms, one pyridine N atom from three HL⁻ ligands and one O atom from SO₄²⁻ [Zn - N 1.958 (2) - 2.010 (2) Å, Zn - O 1.9615 (19) - 1.9907 (19) Å] (**Fig. 1a**, **Fig. S1a** and **Table S1**). The two crystallographically independent ligands HL⁻ are both partially deprotonated, linking three Zn(II) ions via two pyrazol N atoms and one pyridine N atom. The dihedral angles between the triazol ring and two terminal aromatic rings of the two crystallographically independent HL⁻ ligands are 8.9, 8.8, 10.3 and 19.4 °, respectively, indicating the two crystallographically independent HL⁻ ligands are almost planar molecules.

Two Zn(II) ions are linked by two strands of μ_2 - pyrazol bridges into a Zn₂ unit (**Fig. 1a** and **Fig. S1a**). Each Zn₂ unit connects six neighboring Zn₂ units via four HL⁻ ligands and two

SO_4^{2-} anions, thus the Zn_2 unit can be defined as a 6 - connected node with a Schläfli symbol of $(4^{12}, 6^3)$ (Fig. 1a and Fig. S1a). As for the HL⁻ ligand and SO_4^{2-} anion, both of them act as μ_2 -bridges linking two neighboring Zn_2 units, thus they can be considered as 2 - connected nodes and not counted as node topologically (Fig. 1a and Fig. S1a).¹² Topological analysis using TOPOS software indicates complex 1 exhibits a uninodal 6 - connected 2 - fold interpenetrating three - dimensional (3D) architecture with $\{4^{12}, 6^3\}$ - pcu topology (Fig. 1b).¹³

(a)



(b)

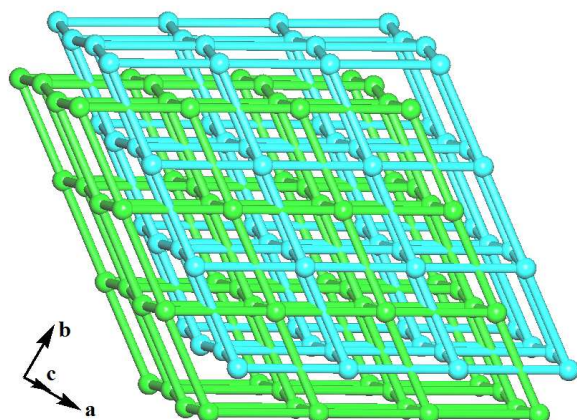


Fig. 1 3D dense architecture constructed by Zn (II), HL⁻ and SO_4^{2-} in complex 1 (H atoms and uncoordinated water molecules omitted for clarity) (a); Schematic illustrating the 2 - fold interpenetrated 3D framework with $\{4^{12}, 6^3\}$ - pcu topology in complex 1 (b).

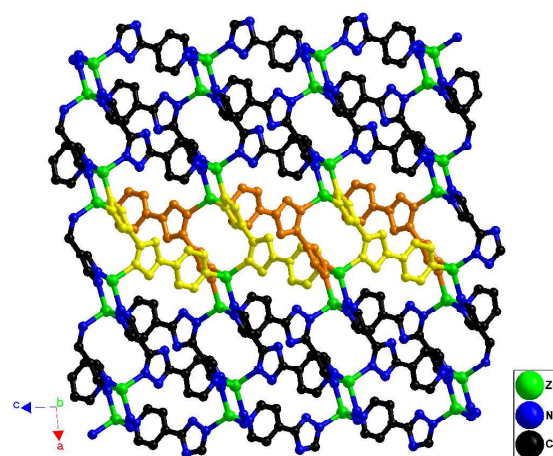
Due to the interpenetration, complex 1 shows a quite dense structure (Fig. S1b) with the pores filled by the coordinated sulphate anions. The solvent - accessible volume of the unit cell of complex 1 is 80.8 \AA^3 , which is occupied by water molecules and is approximately 3.3 % of the unit - cell volume (2441.7 \AA^3).¹¹

When 5 mg complex 1 is immersed in 0.5 M H_2SO_4 (1 mL) aqueous solution, the solid sample can be kept in the solution for two weeks, as shown in Fig. S2a. The PXRD patterns of the samples before and after immersion in H_2SO_4 solution are similar (Fig. S3a), indicating complex 1 is stable in H_2SO_4 solution. As shown in Fig. S3a, it also can be found that the PXRD of the sample after immersion in H_2SO_4 solution shows a significant amorphous hump, indicating the crystal sample utilized for the stability test lost its crystallinity to some extent after immersion in H_2SO_4 solution. The complex possesses low solubility ($1.5 \times 10^{-3} \text{ M}$) in 0.5 M H_2SO_4 aqueous solution, which is probably due to its interpenetrating and quite dense 3D framework. It is estimated that complex 1 is stable in acid and the stability is probably associated with the coordinated SO_4^{2-} in the dense structure, and the quite dense structure is difficult to be

attacked by H_2SO_4 . In an attempt to prove the expectation, another Zn(II) complex formulated as $\text{Zn}_2\text{L}_2 \cdot 12\text{H}_2\text{O}$ (2) was synthesized in the absence of SO_4^{2-} .

Crystal Structure of $\text{Zn}_2\text{L}_2 \cdot 12\text{H}_2\text{O}$ (2) Complex 2 also crystallizes in the monoclinic space group $P2_1/c$ (Table 1), but its asymmetric unit contains one Zn (II), one L^{2-} and six uncoordinated water molecules. No SO_4^{2-} is found in the structure of complex 2. The crystallographically independent L^{2-} is completely deprotonated, linking four Zn (II) ions via two pyrazol N atoms, one triazol N atom and one pyridine N atom with 9.3 and 45.7° of dihedral angles between the triazol ring and two terminal aromatic rings (Fig. 2a and Fig. S4a). Similar to the Zn (II) ions in complex 1, Zn (1) in complex 2 also displays a tetrahedral coordination geometry, but defined by two pyrazol N atoms, one triazol N atom and one pyridine N atom from four L^{2-} ligands [$\text{Zn} - \text{N}$ 1.980 (3) - 2.042 (3) Å] (Fig. 2a, Fig. S4a and Table S1).

(a)



(b)

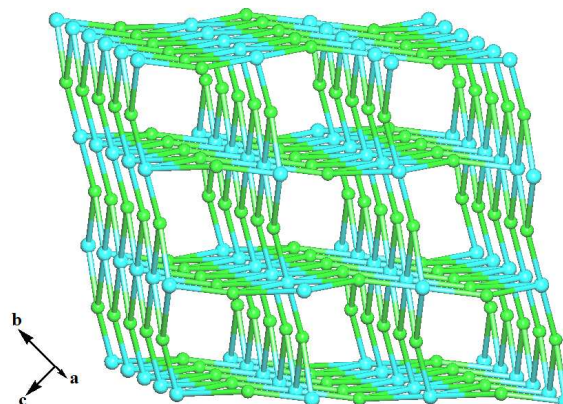


Fig. 2 3D open framework constructed by Zn (II) and L^{2-} in complex 2 (H atoms and uncoordinated water molecules omitted for clarity, two neighboring L^{2-} ligands denoted in different colors for clarity) (a); Schematic illustrating the 3D architecture with $(4, 6)_2(4^2, 6^{10}, 8^3)$ -rtl topology in complex 2 (sapphire nodes, Zn_2 unit; green, L^{2-}) (b).

Similarly, Zn_2 unit is observed in complex 2, which is constructed by two Zn (II) ions and two strands of μ_2 - pyrazol bridges (Fig. 2a and Fig. S4a). Each Zn_2 unit connects six Zn_2 units via six L^{2-} ligands, and the Zn_2 unit functions as a 6 - connected node with a Schläfli symbol of $(4^2, 6^{10}, 8^3)$ (Fig. 2a and Fig. S4a). And the L^{2-} ligand links three neighboring Zn_2 units, it acts as a 3 - connected node with a Schläfli symbol of $(4,$

6²) (Fig. 2a and Fig. S4a).¹³ Topological analysis using *TOPOS* software indicates complex **2** exhibits a 2 - nodal (3, 6)-connected 3D architecture with (4, 6²)₂(4², 6¹⁰, 8³) - *rtl* topology (Fig. 2b).¹³

Herein, complex **2** also displays a 3D extended architecture, however, different from complex **1**, complex **2** displays a more open structure. The solvent - accessible volume of the unit cell of complex **2** is 1166.6 Å³, which is occupied by water molecules and is approximately 57.1 % of the unit - cell volume (2042.8 Å³) (Fig. S4b).¹¹ The XRD powder pattern of complex **2** is shown in Fig. S3b in the ESI. All the peaks of the compound can be indexed to its simulated XRD powder pattern, indicating the sample is in pure phase. When 5 mg complex **2** was immersed in 1 mL of 0.5 M H₂SO₄ aqueous solution, the solid sample was completely decomposed and dissolved into the solution in seconds (Fig. S2b), indicating the instability of the complex in acid. The example further indicates the acid - stability of complex **1** is probably associated with the coordinated SO₄²⁻ in its the dense structure .

Electrochemical Property of Complex 1 Cyclic voltammetry (CV) experiments are performed to evaluate the redox property of complex **1**. In a three-electrode cell, a saturated calomel electrode (SCE) and a platinum foil are used as the reference and counter electrode, respectively. In a 0.5 M H₂SO₄ aqueous solution (50 mL), it is found the CV of the bare glassy carbon electrode (GCE) displays an irreversible wave at -0.15 V in the potential range from -1.5 to 2.0 V at a scan rate of 5 mV·s⁻¹ (Fig. 3 and Fig. S5), which is probably due to the trace impurity in sulphuric acid. In comparison, when the 0.5 M H₂SO₄ solution (50 mL) containing 4 mg H₂L, two couples of quasi-reversible peaks with cathodic peak (E_{pc}) = -0.46 V / anodic peak (E_{pa}) = -0.78 V and E_{pc} = +0.40 V / E_{pa} = -0.11 V, and one irreversible peak at +1.39 V are observed at the bare GCE (Fig. 3 and Fig. S6), which are probably attributed to the redox of aromatic rings of the ligand. Under the same condition, the CV of 4 mg complex **1** modified - glassy carbon electrode (**1** - GCE) shows similar quasi - reversible couple (E_{pc} = +0.32 V / E_{pa} = -0.06 V) and two irreversible peaks at -0.79 and +1.39 V, respectively (Fig. 3 and Fig. S7), they may be related with the redox of the ligand. That is to say, complex **1** has nothing to do with the electrochemistry presented but only the ligand is important for the observed properties. It is also found with the increase of the scan rates, the peak currents increase (Fig. S7).

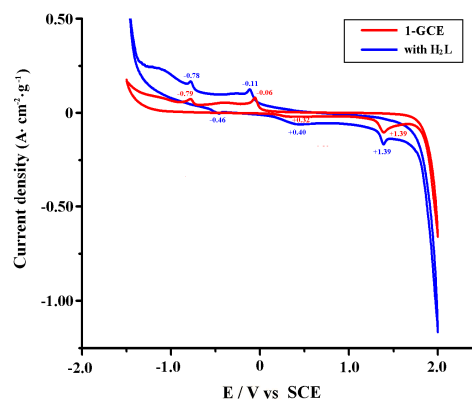
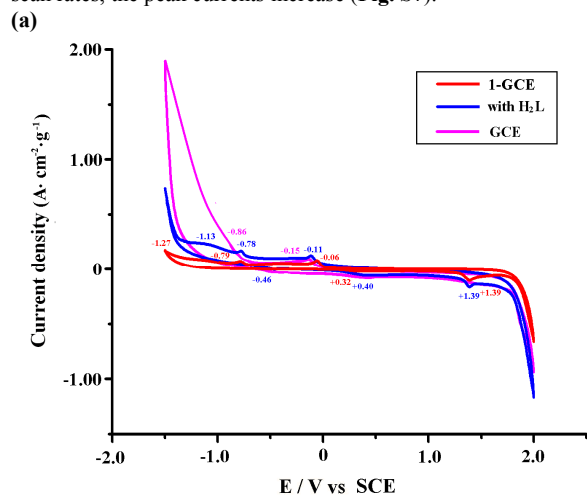


Fig. 3 CVs of the bare GCE (pink) and **1** - GCE (red) in a 0.5 M H₂SO₄ aqueous solution (50 mL) at a scan rate of 5 mV·s⁻¹ with the vertical axis denoted in different scales (a) (b). The blue curve indicates the CV of the bare GCE in the similar solution containing 4 mg H₂L.

As shown in Fig. 3, in the absence and presence of the ligand H₂L, the bare GCE exhibits electrochemical responses with proton reduction at an onset potential of approximately -0.86 and -1.13 V vs SCE, respectively. The irreversible peak for the H₂ evolution reaction (HER) at the **1** - GCE is further negatively shifted to -1.27 V vs SCE with the lowered current, indicating both the ligand H₂L and complex **1** can retard the HER from water. After dozens of CV cycles in the acidic solution in the range from -1.5 to 2.0 V at a scan rate of 50 mV·s⁻¹ (Fig. S7), the solid left on the electrode (denoted as **1a**) was characterized by powder X - ray diffraction (PXRD). **1a** exhibits a PXRD pattern similar to that of complex **1** (Fig. S3), further indicating complex **1** is stable in the acidic solution. The result is also proved by the UV - visible spectrum of **1a** in the H₂SO₄ aqueous solution, which is nearly identical to that of complex **1** (Fig. S8).

Electrodeposition for Complex 1 Recently, electrochemical synthesis based on anodic dissolution has attracted people' attention,^{14,15} which avoids the use of salts and can reduce synthesis time. And the coordination polymer assemble on the anodic surface can be obtained as electrodeposited film instead of brittle crystals via hydro(solvo)thermally technique.¹⁶⁻¹⁸ Herein, in an attempt to electrodeposit complex **1**, 4 mg Zn powder - modified GCE electrode (**Zn** - GCE) was used as working electrode in a 0.5 M H₂SO₄ aqueous solution (50 mL) containing 20 mg H₂L. After several CV cycles in the potential range from -1.5 to 2.0 V at a scan rate of 5 mV·s⁻¹, the color of the grayish **Zn** - GCE (Fig. 4a) was changed accompanying with the generation of bubbles on the electrode, inferring the dissolution of Zn into Zn(II) and the reduction of proton into H₂. Finally, no bubble was observed on the electrode and a layer of white solid sample (denoted as **1b**, yield: ca. 95%) was deposited on the **Zn** - GCE (Fig. 4b).

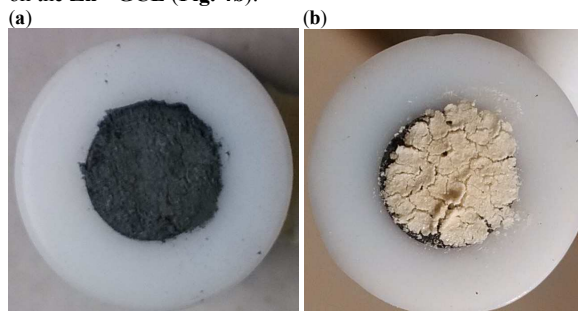
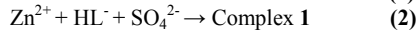


Fig. 4 The images of the **Zn** - GCE before (a) and after CV experiments (b) in a 0.5 M H₂SO₄ aqueous solution (50 mL) containing 20 mg H₂L.

1b exhibits a PXRD pattern similar to that of complex **1** (Fig. S3), indicating complex **1** also can be synthesized via electrodeposition. In our case, it is expected with the proton reduction and the H₂ evolution reaction in the above potential window, the partially deprotonated HL⁻ combined SO₄²⁻ and Zn (II) in the solution into complex **1**, which can be shown as in the following equations:



The H₂SO₄ aqueous solution of **1b** also shows similar UV-visible spectrum to that of complex **1** (Fig. S8). And the CVs of **1b** in a 0.5 M H₂SO₄ aqueous solution (50 mL) are similar to those of complex **1** under the same condition (Fig. S9), which further proves the formation of complex **1** on the electrode via the electrodeposition technique.

In comparison, the CVs of the Zn - GCE in the 0.5 M H₂SO₄ solution in the absence of H₂L ligand were measured. As shown in Fig. 5, Fig. S10 and Fig. S11, the CVs of the Zn - GCE are different from that of **1** - GCE. And the peak potentials for the Zn dissolution at a scan rate of 50 mV·s⁻¹ in the presence and absence of H₂L for the initial several cycles are -0.30 and -0.73 V, respectively. The potential of Zn corrosion is positively shifted and the corrosion current is much enhanced in the presence of H₂L with respect to the blank system (Fig. 4), indicating the presence of H₂L can prompt the oxidation of Zn into Zn (II). It is probably due to the formation of complex **1**, as shown in equation 2, equation 1 is more liable on the view of equilibrium.

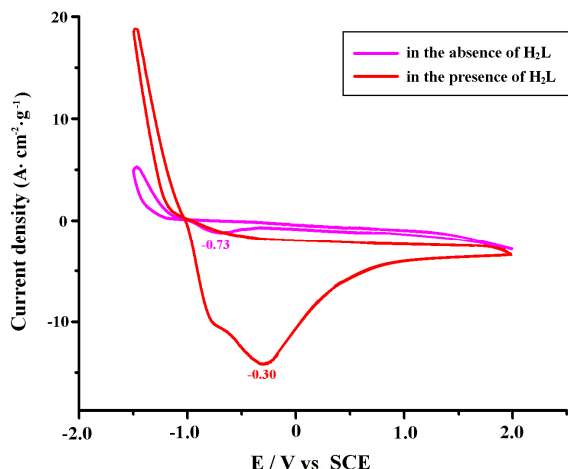
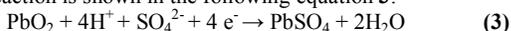


Fig. 5 Comparison of CVs at the Zn - GCE scanned from -1.5 to 2.0 V in 0.5 M H₂SO₄ aqueous solution (50 mL) in the absence (pink) and presence of 20 mg H₂L (red) at a scan rate of 50 mV·s⁻¹.

The Effect of Complex 1 on Zn - PbO₂ Battery Over the next 20 years, energy storage will be a key technology for global energy sustainability. Out of a variety of energy storage types, battery is still one of the most promising. In the presence of work, in an attempt to investigate the electrochemical mechanism of Zn - PbO₂ battery, we investigate its discharge properties in the absence and presence of H₂L. As we know, the electrochemical reaction of the negative electrode in a Zn - PbO₂ battery is shown in the above equation 1. And the positive reaction is shown in the following equation 3:



Herein, the galvanostatic discharge curves were measured in a two - electrode cell, in which the 4 mg Zn modified GCE (Zn - GCE) and 4 mg PbO₂ powder modified GCE (PbO₂ - GCE) were used as negative and positive electrodes, respectively (Fig. S12). And the 0.5 M H₂SO₄ aqueous solution (50 mL) was used as electrolyte.

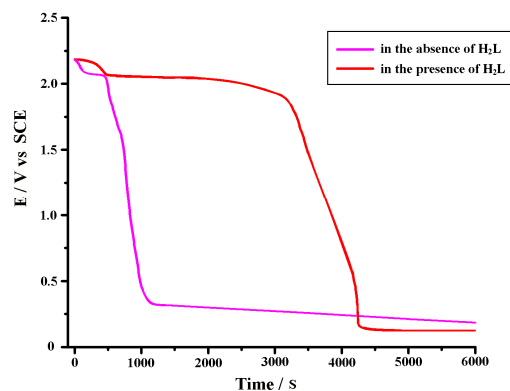


Fig. 6 Discharge curves of the Zn - PbO₂ batteries in the absence and presence of 20 mg H₂L at a current of 0.125 A·g⁻¹ under room temperature. Supporting electrolyte = 0.5 M H₂SO₄ aqueous solution (50 mL).

Fig. 6 shows the discharge characteristics of the Zn - PbO₂ batteries at a current of 0.125 A·g⁻¹ in the absence and presence of 20 mg H₂L under room temperature. It is found the electromotive forces (*E*) of the batteries in the absence and presence of the ligand are approximately 2.2 V (Fig. 6). As we know, *E*⁰(Zn²⁺/Zn) = -0.76 V, *E*⁰(PbO₂/PbSO₄) = 1.69 V, thus the standard electromotive force (*E*⁰) of the battery is 2.45 V, which is slightly higher than the measured values. As shown in Fig. 6, the galvanostatic discharge curves of the batteries show two discharge plateaus. The first plateau voltage is approximately 2 V, and the second discharge plateau is below 0.5 V. The discharge times of the batteries at 2 V in the presence and absence of H₂L are approximately 3200 and 500 s, respectively (Fig. 6). The former discharging time is much longer than the latter. It is speculated that the phenomenon is associated with the formation of complex **1** in the presence of the ligand during the discharging process. If the Zn - GCE is covered by the film of complex **1**, which protects the fast dissolution of the anode, long discharging time is obtained.

The images of the Zn - GCE in the Zn - PbO₂ battery before and after the discharge experiment in the absence and presence of H₂L are shown in Fig. S13. It is found that the morphologies of the Zn - GCE after the discharge experiment in the absence and presence of H₂L are different. The compound (denoted as **1c**) left on the Zn - GCE in the presence of H₂L after the discharge experiment is characterized by UV - vis absorption spectrum. As shown in Fig. S14, **1c** and **1** show similar UV absorption peaks at 284 and 285 nm in the range of 240 - 600 nm, which is completely different from the UV - vis absorption spectrum of the Zn powder, indicating complex **1** is probably formed on the Zn - GCE in the presence of H₂L during the discharge course.

Thermal Stabilities of Complexes 1 and 2 In order to examine the thermal stabilities of complexes **1** and **2**, thermogravimetric analyses (TGAs) were carried out. The samples were heated up to 750 °C in N₂. As shown in Fig. S15, complex **1** shows a one step weight loss of 3.0 % in the range of 20 - 180 °C corresponding to the loss of the lattice water molecules (calc. 2.7 wt %). The anhydrous sample remained stable up to ~290 °C without any weight loss. As shown in Fig. S15, complex **1b** shows similar TG curve to complex **1**, further indicating complexes **1b** and **1** probably possess similar structure.

It is found that the cavity of complex **2** is occupied by six molecules per unit, as estimated by SQUEEZE and TGA.¹¹ As shown in Fig. S15, complex **2** releases its uncoordinated water molecules in the range of 30 - 220 °C with a loss of 28.5 wt %

(calc. 28.2 wt %). And the decomposition of the organic ligand began at 470 °C.

Conclusion

In conclusion, two Zn (II) complexes formulated as $Zn_2(HL)_2(SO_4) \cdot H_2O$ (**1**) and $Zn_2L_2 \cdot 12H_2O$ (**2**) have been synthesized and structurally characterized by single - crystal X - ray diffraction. Complex **1** features a uninodal 6 - connected 2 - fold interpenetrating 3D dense architecture with $\{4^{12} \cdot 6^3\}$ - **pcu** topology, and complex **2** exhibits a 2 - nodal (3, 6) - connected 3D open architecture with $(4 \cdot 6^2)_2(4^2 \cdot 6^{10} \cdot 8^3)$ - **rtf** topology. However, complex **1** is stable in sulfuric acid, and complex **2** is not. The example indicates the acid - stability of complex **1** is probably associated with the coordinated SO_4^{2-} in the dense structure. Furthermore, complex **1** can be synthesized via electrodeposition in sulfuric acid during the CV experiment. It is expected that due to the formation of the film of complex **1** on the Zn electrode, the discharging time of the Zn - PbO_2 battery in the presence of H_2L is longer than that in the absence of H_2L under room temperature. The detailed mechanism is under way.

Supporting Information

Crystallographic data; PXRD patterns; CVs; UV - vis absorption spectra; TG curve and other supplementary material are included in the supporting information. This information is available free of charge via the Internet at <http://pubs.rsc.org/>.

Financial supports from the National Natural Science Foundation of China (No. 21371184), the Fundamental Research Funds for the Central Universities (No. CQDXWL - 2012 - 024) and Chongqing Key Laboratory of Chemical Process for Clean Energy and Resource Utilization are gratefully acknowledged.

References

- (a) J. R. Long, O. M. Yaghi, *Chem. Soc. Rev.* **2009**, *38*, 1213-1214; (b) T. Uemura, N. Yanai, S. Kitagawa, *Chem. Soc. Rev.* **2009**, *38*, 1228-1236; (c) J. Y. Lee, O. K. Farha, J. Roberts, K. A. Scheidt, S. T. Nguyen, J. T. Hupp, *Chem. Soc. Rev.* **2009**, *38*, 1450-1459; (d) J. R. Li, R. J. Kuppler, H. C. Zhou, *Chem. Soc. Rev.* **2009**, *38*, 1477-1504; (e) L. Ma, C. Abney, W. B. Lin, *Chem. Soc. Rev.* **2009**, *38*, 1248-1256; (f) L. J. Murray, M. Dinca, J. R. Long, *Chem. Soc. Rev.* **2009**, *38*, 1294-1314; (g) O. K. Farha, A. O. Yazaydin, I. Eryazici, C. D. Malliakas, B. G. Hauser, M. G. Kanatzidis, S. T. Nguyen, R. Q. Snurr, J. T. Hupp, *Nat. Chem.* **2010**, *2*, 944-948; (h) B. Yuan, Y. Pan, Y. Li, B. Yin, H. Jiang, *Angew. Chem. Int. Ed.* **2010**, *49*, 4054-4058.
- M. Eddaoudi, J. Kim, N. Rosi, D. Vodak, J. Wachter, M. O'Keeffe, O. M. Yaghi, *Science* **2002**, *295*, 469-472.
- a) Y. Li, R. T. Yang, *Langmuir* **2007**, *23*, 12937-12944; b) D. Ma, Y. Li, Z. Li, *Chem. Commun.* **2011**, *47*, 7377-7379; c) J. Yang, A. Grzech, F. M. Mulder, T. J. Dingemans, *Chem. Commun.* **2011**, *47*, 5244-5246; d) H. J. Choi, M. Dinca, A. Dailly, J. R. Long, *Energy Environ. Sci.* **2010**, *3*, 117-123. e) S. S. Kaye, A. Dailly, O. M. Yaghi, J. R. Long, *J. Am. Chem. Soc.* **2007**, *129*, 14176-14177; f) C. R. Wade, T. Corrales-Sanchez, T. C. Narayan, M. Dinca, *Energy Environ. Sci.* **2013**, *6*, 2172-2177.
- a) J. H. Cavka, S. Jakobsen, U. Olsbye, N. Guillou, C. Lamberti, S. Bordiga, K. P. Lillerud, *J. Am. Chem. Soc.* **2008**, *130*, 13850-13851; b) D. W. Feng, Z. Y. Gu, J. R. Li, H. L. Jiang, Z. W. Wei, H. C. Zhou, *Angew. Chem. Int. Ed.* **2012**, *124*, 10453-10456.
- G. Ferey, C. Mellot-Draznieks, C. Serre, F. Millange, J. Dutour, S. Surble, I. Margiolaki, *Science* **2005**, *309*, 2040-2042.
- a) R. Banerjee, A. Phan, B. Wang, C. Knobler, H. Furukawa, M. O'Keeffe, O. M. Yaghi, *Science* **2008**, *319*, 939-943; b) C. Y. Sun, C. Qin, X. L. Wang, G. S. Yang, K. Z. Shao, Y. Q. Lan, Z. M. Su, P. Huang, C. G. Wang, E. B. Wang, *Dalton Trans.* **2012**, *41*, 6906-6909.
- J. J. Low, A. I. Benin, P. Jakubczak, J. F. Abrahamian, S. A. Faheem, R. R. Willis, *J. Am. Chem. Soc.* **2009**, *131*, 15834-15842.
- V. Niraimathi, V. Vaidhyalingam, A. Aruna, A. Vadivelu, *Acta Cienc. Indica Chem.* **2009**, *35*, 43-48.
- V. Niraimathi, V. Vaidhyalingam, A. Aruna and A. Vadivelu, *Acta Cienc. Indica, Chem.*, **2009**, *35*, 43-48.
- (a) G. M. Sheldrick, *SHELXS 97, Program for Crystal Structure Solution*, University of Göttingen, Göttingen, Germany, **1997**; (b) G. M. Sheldrick, *SHELXL 97, Program for Crystal Structure Refinement*, University of Göttingen, Göttingen, Germany, **1997**.
- (a) A. L. Spek, *J. Appl. Crystallogr.* **2003**, *36*, 7-13; (b) X. F. Wang, Y. B. Zhang, H. Huang, J. P. Zhang and X. M. Chen, *Cryst. Growth Des.*, **2008**, *8*, 4559-4563.
- O. D. Friedrichs, M. O'Keeffe, O. M. Yaghi, *Acta Crystallogr. A* **2003**, *59*, 22-27.
- V. A. Blatov, *IUCr CompComm. Newsl.* **2006**, *7*, 4, published online Nov, 2006. See also <http://www.topos.ssu.samara.Ru>.
- R. Ameloot, L. Stappers, J. Fransaer, L. Alaerts, B. F. Sels, D. E. De Vos, *Chem. Mater.* **2009**, *21*, 2580-2582.
- A. Martinez Joaristi, J. Juan-Alcaniz, P. Serra-Crespo, F. Kapteijn, J. Gascon, *Cryst. Growth Des.* **2012**, *12*, 3489-3498.
- M. Y. Li, M. Dincă, *Chem. Sci.* **2014**, *5*, 107-111.
- N. Campagnol, T. V. Assche, T. Boudewijns, J. Denayer, K. Binnemans, D. De Vos, J. Fransaer, *J. Mater. Chem. A* **2013**, *1*, 5827-5830.
- M. Y. Li, M. Dincă, *J. Am. Chem. Soc.* **2011**, *133*, 12926-12929.

